Electronic Supplementary Information

Experimental Section

Synthesis of the NiCo-MOF/NF

Prior to the preparation, the nickel foam (NF) was ultrasonic cleaned successively with acetone (30 min), deionized water (1 h) and anhydrous ethanol (1 h). Generally, 0.3172 g $CoCl_2·6H_2O$, 0.1585 g $NiCl_2·6H_2O$ and 0.1660 g Terephthalic acid (PTA) were dissolved in 35 mL N,N-dimethylformamide (DMF), 2.5 mL anhydrous ethanol and 2.5 mL deionized water, and stirred for 30 min. Subsequently, the above mixed solution was transferred to a 50 mL reaction kettle, and a piece of previously prepared NF was added. The reaction was carried out at 125 °C for 12 h. After reaction, the obtained NiCo-MOF/NF precursor was washed with water and ethanol for 3 times, and dried at 60 °C in vacuum for 12 h.

Synthesis of the $NiCo_2O_4$/NF

The NiCo-MOF/NF precursor was transformed into $NiCo_2O_4$/NF by annealing at 300 °C in air atmosphere for 2 h with the heating rate of 2 °C min^{-1}. The mass loading of $NiCo_2O_4$ on NF was about 3.2 mg cm^{-2}.

Synthesis of x-O_v-$NiCo_2O_4$/NF

The $NiCo_2O_4$/NF was immersed into deionized water (40 mL) containing different amounts of $NaBH_4$ (0.06, 0.1, 0.2, 0.3M) for 2 h at room temperature to induce oxygen vacancies, and the samples were denoted as x-O_v-$NiCo_2O_4$/NF (x corresponded to molar concentration of $NaBH_4$). The sample was washed with water

and dried at 60 °C for 12 h. The mass loading of 0.1-O_v-$NiCo_2O_4$ was around 2.8 mg cm^{-2}.

Characterization

X-ray diffraction (XRD) patterns were collected from a Bruker AXS D8 Advance X-ray diffractometer with Cu Kα radiation (λ=1.5406Å). Scanning electron microscopy (SEM, Hitachi S-4800) was used to observe the surface morphology of the samples. The micro-structure and elemental compositions of the samples were studied by transmission electron microscopy (TEM, JEOL JEM 2100) and energy dispersive X-ray spectroscopy (EDS, Oxford X-max). X-ray photoelectron spectroscopy (XPS) measurements were performed on a Thermo Scientific ESCA-Lab-200i-XL spectrometer. Atomic force microscope (AFM) image was obtained using Bruke Dimension Icon. Electron paramagnetic resonance (EPR) spectra were recorded with Bruker EPR EMXPLUS 10/12 spectrometer at room temperature.

Electrochemical measurements

The electrochemical properties of as-prepared electrodes were tested in a three-electrode cell containing 2 M KOH electrolyte at room temperature. $NiCo_2O_4$/NF or O_v-$NiCo_2O_4$/NF was directly used as working electrode, a platinum wire was used as the counter electrode and a saturated calomel electrode (SCE) was acted as the reference electrode. Cyclic voltammetry (CV), galvanostatic charge-discharge (GCD) and electrochemical impedance spectroscopy (EIS) tests were carried out by a CHI 660E electrochemical workstation (Shanghai chenhua). The specific capacitance of the supercapacitor was calculated by the following formula:

$$C_a = \frac{2I}{S \times \Delta V} \int_0^{\Delta t} V dt \qquad (S1)$$

where C_a (F cm^{-2}) was the areal capacitance, I (A) was the discharge current, Δt (s) was the total discharge time, A (cm^2) was the active electrode area, and ΔV (V) was the potential of the charge-discharge process.

A two-electrode asymmetric supercpacitor (ASC) device was assembled in 2 M KOH electrolyte by using the 0.1-O_v-NiCo$_2$O$_4$/NF and an AC electrode as positive and negative electrodes, respectively. In order to achieve charge balance between both electrodes, the mass ratio of 0.1-O_v-NiCo$_2$O$_4$/NF to AC was optimized on the basis of following equation:

$$\frac{m_+}{m_-} = \frac{C_- \times \Delta V_-}{C_+ \times \Delta V_+} \qquad (S2)$$

where m (g), C (F g^{-1}) and ΔV (V) were the mass, specific capacitance and discharge potential window of positive and negative electrodes. The energy density (E, Wh kg^{-1}) and power density (P, W kg^{-1}) of the ASC were calculated as follows:

$$E = \frac{C_s \times (\Delta V)^2}{2 \times 3.6} \qquad (S3)$$

$$P = \frac{3600E}{\Delta t} \qquad (S4)$$

where C_s (F g^{-1}) was the specific capacitance of the ASC, ΔV (V) was the working voltage window of the ASC, and Δt (s) was the discharge time of the ASC.
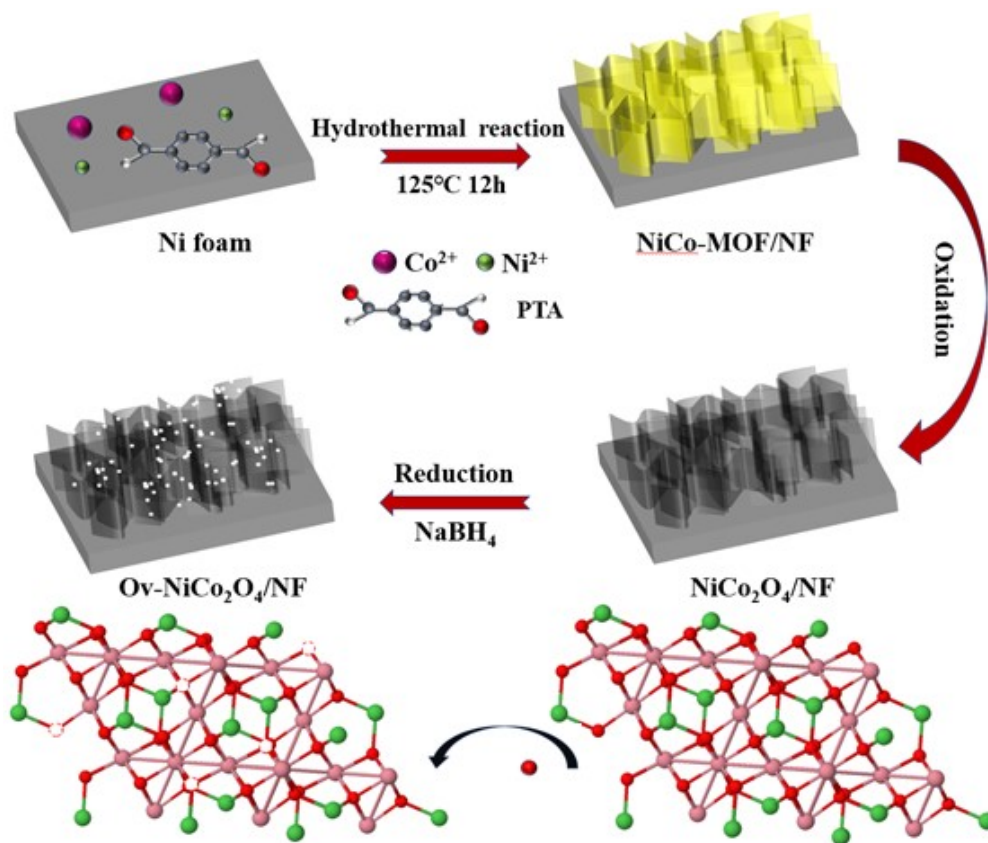
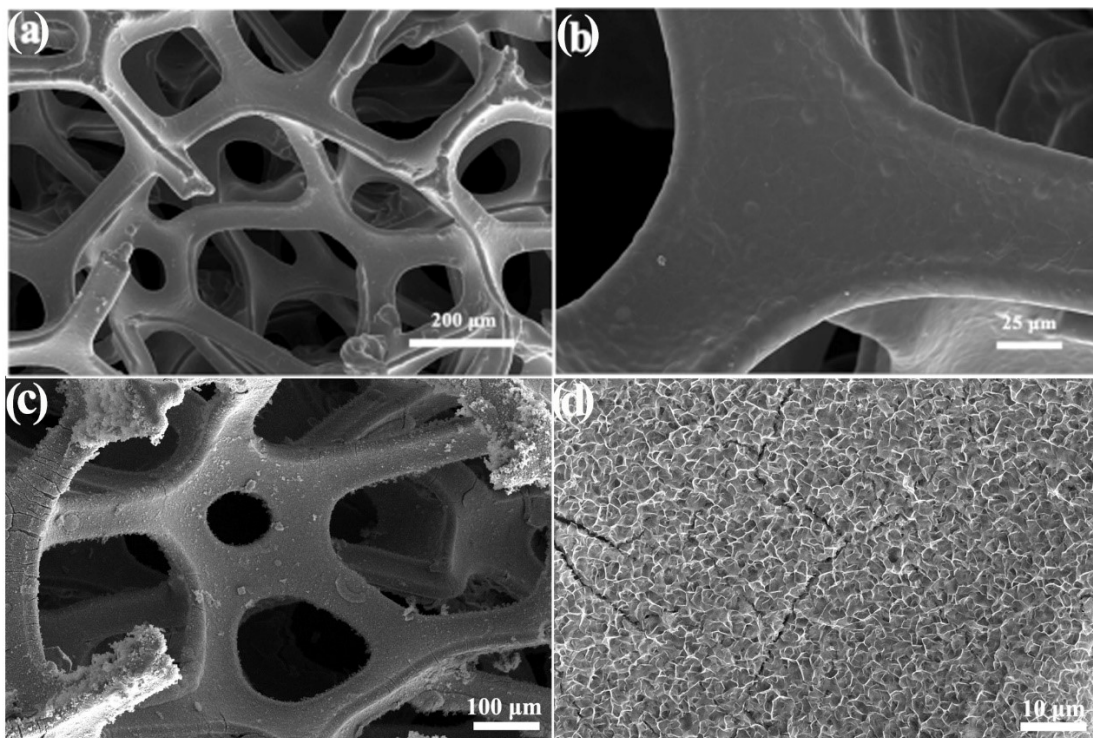Fig. S1 Schematic illustration of construction of the O_v-NiCo$_2$O$_4$/NF.

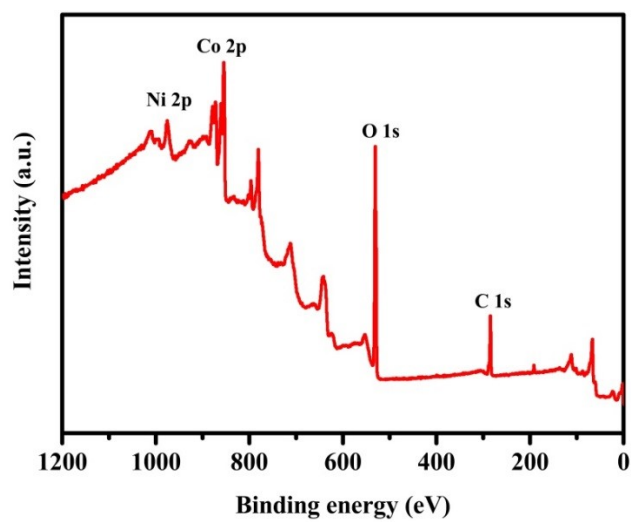**Fig. S2** SEM images of (a, b) bare Ni foam and (c, d) NiCo-MOF at different magnifications.
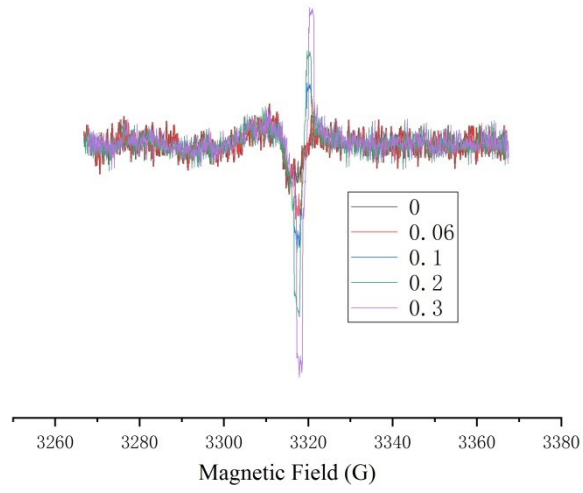
Fig. S3 XPS survey spectrum of the 0.1-O_v-NiCo$_2$O$_4$/NF.

Fig. S4. EPR spectra of the NiCo$_2$O$_4$ and x-Ov-NiCo$_2$O$_4$.
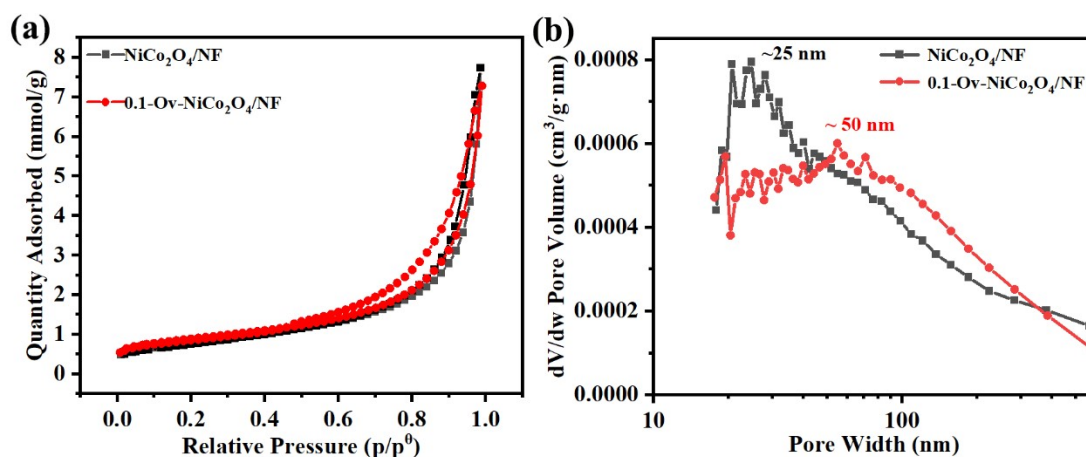
Fig. S5. (a) Nitrogen physisorption isotherms and (b) the corresponding pore size distributions of $NiCo_2O_4/NF$ and $0.1-O_v-NiCo_2O_4/NF$.

The samples display the typical IV isotherm with H_3 type hysteresis, implying that the sample contains mesopores. The specific surface area of $0.1-Ov-NiCo_2O_4/NF$ (67.99 m^2 g^{-1}) is larger than that of $NiCo_2O_4/NF$ (61.34 m^2 g^{-1}). Due to the introduction of oxygen vacancy, the pore size and specific surface area of the material are increased. The large specific surface area will expose more electroactive sites, which is conducive to faradaic redox reactions.
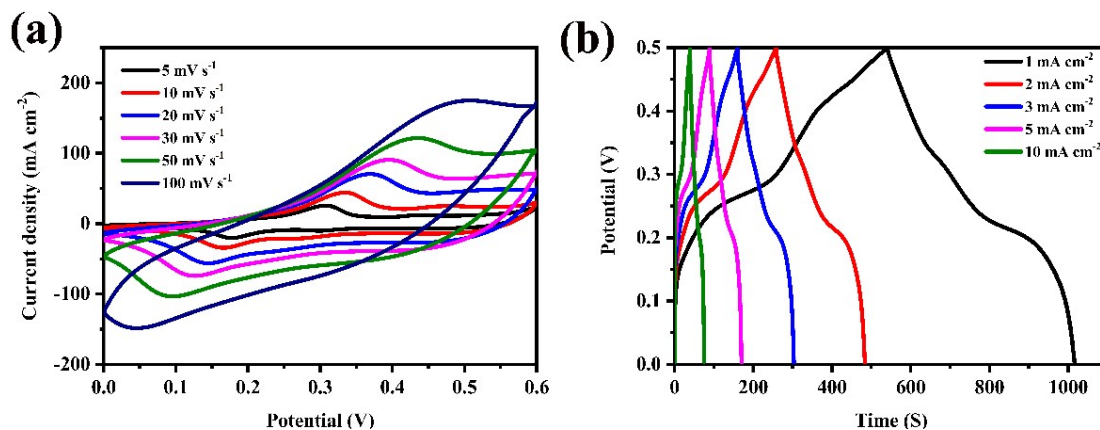
Fig. S6 Electrochemical performance of the 0.1-O_v-$NiCo_2O_4$/NF electrode. (a) CV curves at different scan rates and (b) GCD curves at various current densities.

It can be seen that the overall shape of CV curve basically remains unchanged with the increase of scanning rate, reflecting its good rate performance. Its GCD curves show good symmetry, indicating that the electrode material has a high Columbic efficiency and good electrochemical reversibility.
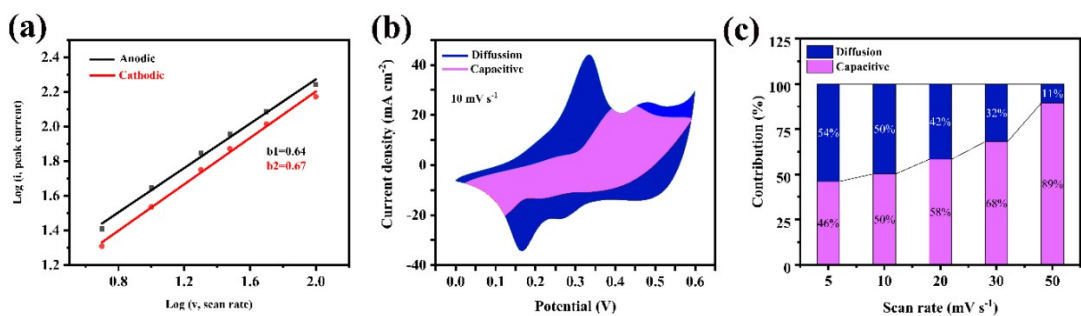
Fig. S7 Analysis of charge storage mechanism of 0.1-O_v-NiCo$_2$O$_4$/NF electrode. (a) Logarithm of peak currents of as a function of logarithm of scan rates. (b) CV curve at 10 mV s^{-1} showing the contributions of capacitive and diffusion-controlled processes. (c) The relative proportions of diffusion-controlled and capacitive processes as a function of scan rate.

The charge storage mechanism of the 0.1-O_v-NiCo$_2$O$_4$/NF electrode was further investigated by analyzing the CV curves. The relationship between current (i) and scan rate (v) can be expressed by following equation.

$$i = av^b \text{ (S5)}$$

The electrochemical energy storage is classified into two different processes depending on the b-values. When b=1, it means that the charge storage is capacitive, while b=0.5, it means that charge storage is diffusion-controlled. By linear fitting log (i) vs. log (v), b-values are obtained from the slopes of the fitted lines. The b values are 0.64 and 0.67 for the cathodic and anodic processes (Fig. S6a), indicating that both processes contribute to the current response. In addition, the proportions of diffusion-controlled and capacitive processes are further calculated according to the following equation:

$$i\ (V) = k_1 \upsilon + k_2 \upsilon^{1/2} \quad \text{(S6)}$$

Fig. S6b depicts a typical CV curve, distinguishing the contributions of capacitive and diffusion-controlled processes. As the scan rate increases from 5 to 50 mV s^{-1} (Fig. S6c, the contribution of the diffusion-controlled process decreases from 54 to 11%.
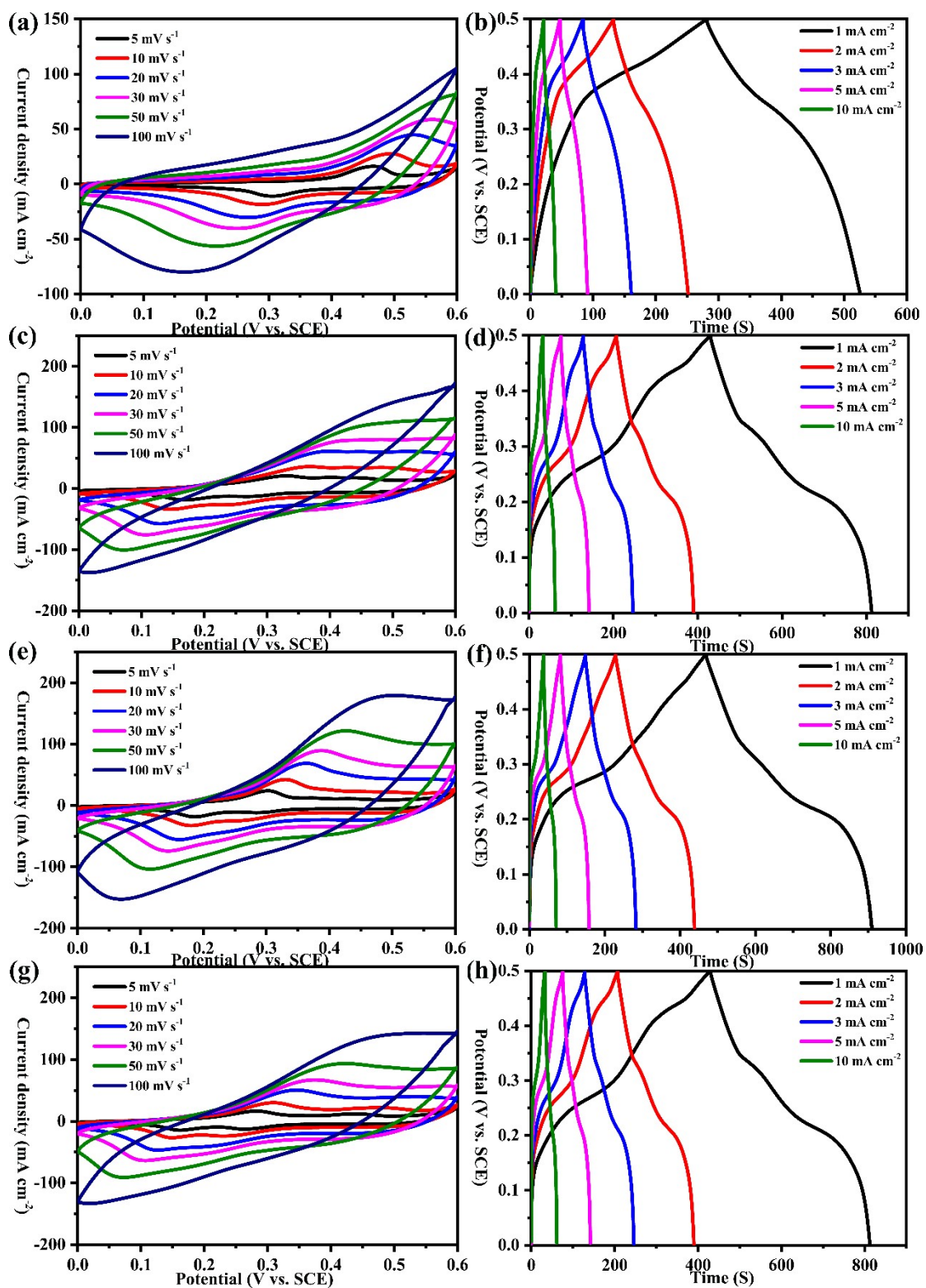
Fig. S8 (a, c, e, g) CV and (b, d, f, h) GCD curves of (a, b) $NiCo_2O_4$/NF, (c, d) 0.06-O_v-$NiCo_2O_4$/NF, (e, f) 0.2-O_v-$NiCo_2O_4$/NF and (g, h) 0.3-O_v-$NiCo_2O_4$/NF.
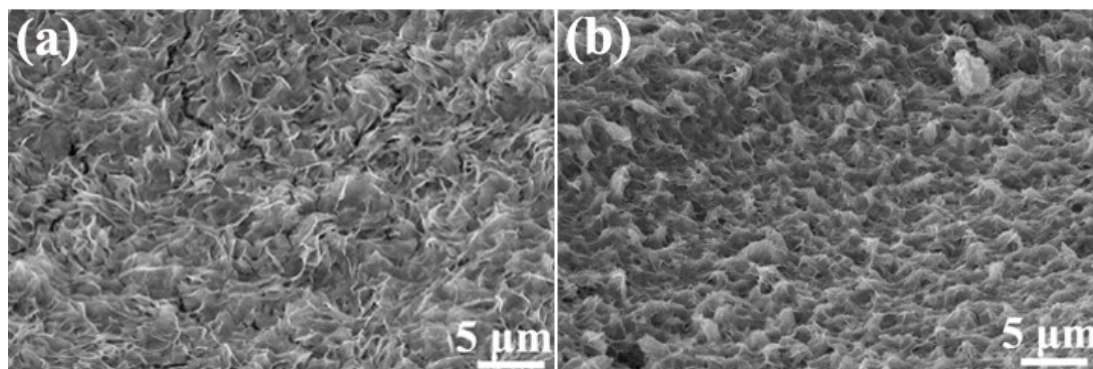
Fig. S9 SEM images of the (a) 0.2-O_v-NiCo$_2$O$_4$/NF and (b) 0.3-O_v-NiCo$_2$O$_4$/NF.
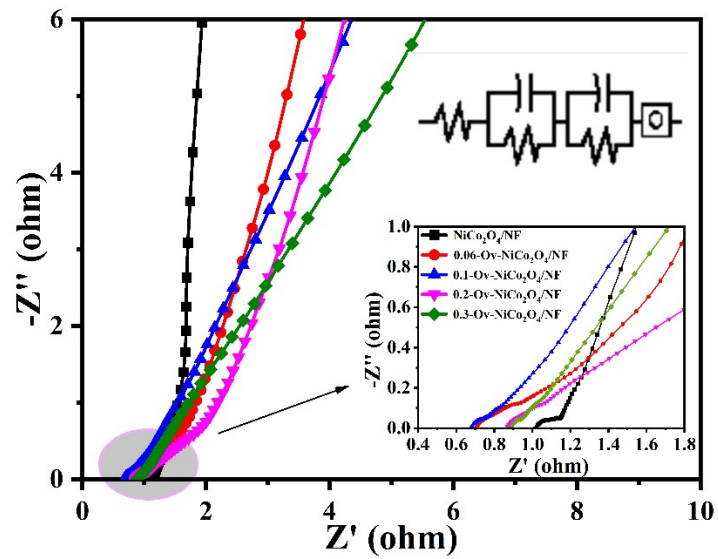
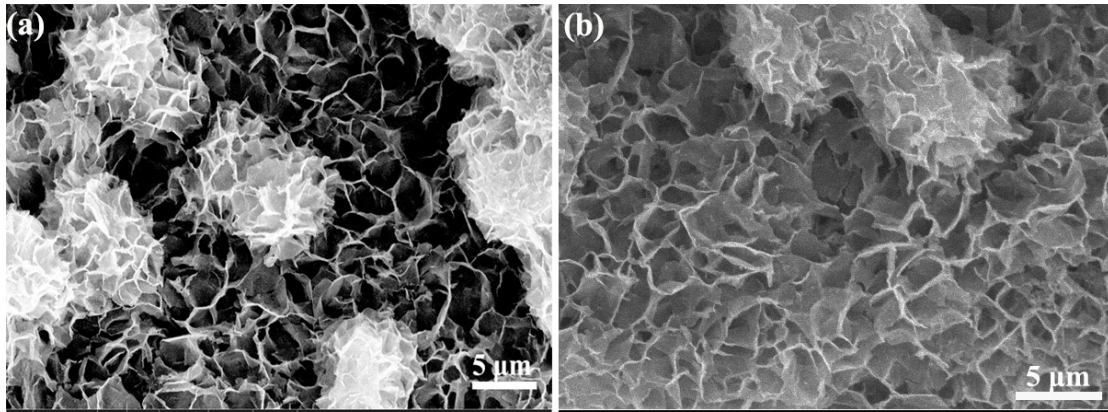**Fig. S10** Nyquist plots of the NiCo$_2$O$_4$/NF and x-O$_v$-NiCo$_2$O$_4$/NF electrodes.

Fig. 11 SEM images of 0.1-Ov-NiCo2O4/NF (a) before and (b) after 5000 cycles.

The SEM image of the electrode after cycling suggests that the initial structure of the electrode material is basically maintained.
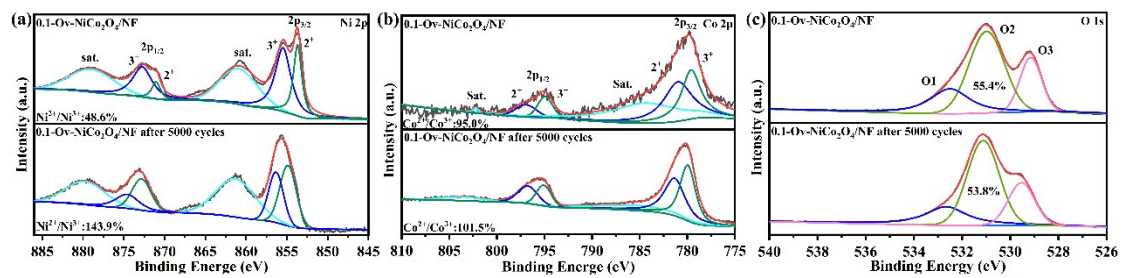

Fig.12 High-resolution XPS spectra of the 0.1-O_v-NiCo$_2$O$_4$/NF before and after 5000 cycles scraped from NF in the (a) Ni 2p, (b) Co 2p, and (c) O 1s regions.
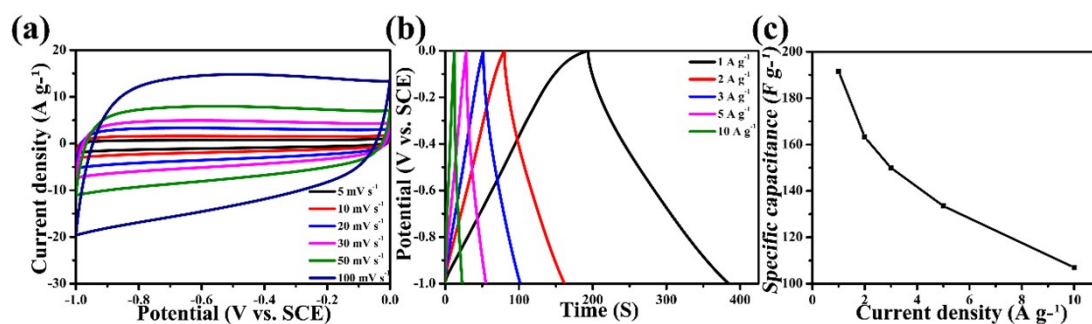
Fig. S13 (a) CV curves at different sweep rates, (b) GCD curves at various current densities and (c) specific capacitances calculated by the GCD curves of the AC electrode.

Before constructing the ASC device, the electrochemical performance of a single AC was carried out. The rectangular CV curves and the triangular GCD curves imply the electrochemical behavior of electric double layer capacitors (EDLCs). The AC electrode can display a high specific capacitance of 197.7 F g^{-1} at 1 A g^{-1}. Thus, according to the charge balance (Eq. S2), the optimal mass ratio of 0.1-O$_v$-NiCo$_2$O$_4$ to AC is calculated to be1.13:1.
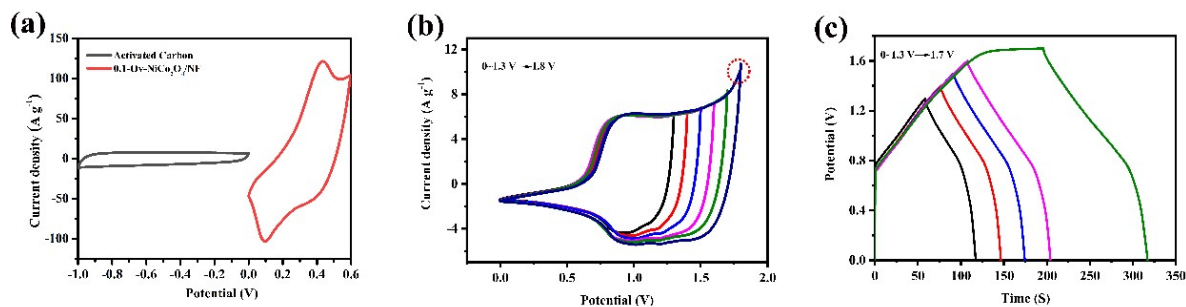
Fig. S14 (a) CV curves of individual AC and 0.1-Ov-NiCo$_2$O$_4$/NF at 50 mV s^{-1}. (b) CV curves of the 0.1-O$_v$-NiCo$_2$O$_4$/NF//AC at different voltage windows at 50 mV s^{-1}. (c) GCD curves of the 0.1-Ov-NiCo$_2$O$_4$/NF//AC at different voltage windows at 1 A g^{-1}.

The AC and 0.1-O$_v$-NiCo$_2$O$_4$/NF electrodes work stably in separated potential window of -0.1-0 V (vs. SCE) and 0-0.6 V (vs. SCE), respectively. Therefore, the working voltage of the assembled 0.1-Ov-NiCo$_2$O$_4$/NF//AC should be extended to around 1.6 V. To optimize the operating voltage of ASC, a series of CV and GCD curves at different voltage winnowed were collected. As shown in Fig. S11b, obvious oxygen evolution occurs at a voltage of 1.8 V, while GCD (Fig. S11c) shows that the stable working voltage of ASC can be extended to 1.7 V. Therefore, 1.7 V was chosen as the working voltage for further electrochemical studies.